Motion and collision of particles in a rotating linear dilaton black hole

P. A. González,[1,*] Marco Olivares,[1,†] Eleftherios Papantonopoulos,[2,‡] and Yerko Vásquez[3,§]
[1]*Facultad de Ingeniería y Ciencias, Universidad Diego Portales, Avenida Ejército Libertador 441, Casilla 298-V Santiago, Chile*
[2]*Department of Physics, National Technical University of Athens, Zografou Campus GR 157 73, Athens, Greece*
[3]*Departamento de Física y Astronomía, Facultad de Ciencias, Universidad de La Serena, Avenida Cisternas 1200, La Serena, Chile*

(Received 14 February 2018; published 26 March 2018)

We study the motion of particles in the background of a four-dimensional linear dilaton black hole. We solve analytically the equations of motion of the test particles, and we describe their motion. We show that the dilaton black hole acts as a particle accelerator by analyzing the energy in the center of mass frame of two colliding particles in the vicinity of its horizon. In particular, we find that there is a critical value of the angular momentum, which depends on the string coupling, and a particle with this critical angular momentum can reach the inner horizon with an arbitrarily high c.m. energy. This is known as the Bañados, Silk, and West process. We also show that the motion and collisions of particles have behavior similar to the three-dimensional Bañados-Teitelboim-Zanelli black hole. In fact, the photons can plunge into the horizon or escape to infinity, and they cannot be deflected, while for massive particles there are no confined orbits of the first kind, like planetary or circular orbits.

DOI: 10.1103/PhysRevD.97.064034

I. INTRODUCTION

Stringy black holes are interesting because they have quite different properties from those that appear in the black hole solutions of general relativity (GR). The main ingredient of these solutions is the presence of a scalar field, the dilaton, which effectively acts as a string coupling. Then, with a suitable conformal transformation, this field couples to the electromagnetic field, and this new coupling alters the known properties of spherically symmetric black hole solutions of GR. A static stringy charged black hole solution was found in Ref. [1], and independently in Ref. [2], known as the Garfinkle-Horowitz-Strominger (GHS) black hole. These solutions resulted from a four-dimensional field theory of a heterotic string theory. Then, in the context of the heterotic string theory, a general electrically charged, rotating black hole solution was found [3,4] and was later was extended [5], and black hole solutions were found carrying electric charge, and both electric and magnetic types antisymmetric tensor gauge field charge. Also, solitonic black hole solutions [6] and black hole solutions in the presence of a cosmological constant [7] were found.

In Ref. [8], within the Einstein-Maxwell-dilaton-axion theory, rotating black hole solutions which asymptote to the linear dilaton spacetime were found. The nonrotating case can be considered as some limit of extremal GHS black holes with a geometric interpretation of a horizon plus a throat describing a nonasymptotically flat black hole. Particularly, they can be regarded as excitations over the linear dilaton vacua, forming a two-parameter family, which can be obtained as near-horizon and near-extreme limits of the parent dilaton black holes. Also, in Ref. [8], a rotating version of linear dilaton black holes in which the dilaton field is independent of the black hole mass was found. The metric possesses an ergosphere outside the event horizon, which rotates with some angular velocity Ω_h. The angular momentum J computed as a surface integral at spatial infinity contains both a geometrical contribution and that coming from the Maxwell field. The Hawking temperature and the entropy depend on both the mass and the angular momentum of the black hole; these quantities are shown to satisfy the first law in the form $d\mathcal{M} = TdS + \Omega_h dJ$. Also, analytical solutions of rotating linear dilaton black holes were discussed in Refs. [9,10].

The Hamilton-Jacobi equation in the rotating linear dilaton black hole spacetime is shown to be separable [8] as in the Kerr case, indicating the existence of a Stachel-Killing tensor. Timelike geodesics do not escape to infinity, while null ones do so for an infinite affine parameter. The Klein-Gordon equation is also separable; the mode behavior near the horizon exhibits the superradiance phenomenon. It was shown that all superradiant modes are reflected at large distances from the black hole, so there is no

*pablo.gonzalez@udp.cl
†marco.olivaresr@mail.udp.cl
‡lpapa@central.ntua.gr
§yvasquez@userena.cl

superradiant flux at infinity, in contrast with the case of massless fields in the Kerr spacetime. This situation is similar to the confinement of *massive* superradiant modes in the Kerr metric, which are reflected back to the horizon, causing stimulated emission and absorption. In the classical limit, this leads to an amplification effect due to the positive balance between emission and absorption. In the Kerr spacetime, this phenomenon is rather small, being present only for massive modes. In our case, massless modes are confined, too; therefore, all superradiant modes will form a cloud outside the horizon with an exponentially growing amplitude. This is in fact a classical instability which manifests itself in the rapid transfer of angular momentum from the hole to the outside matter cloud. A similar conclusion was obtained in Ref. [11] for the case of the Kerr–anti-de Sitter (AdS) spacetime with reflecting boundary conditions on the AdS boundary. The stability of the rotating linear dilationic black hole was also studied in Ref. [12] by calculating the quasinormal modes of scalar field perturbations and superradiant modes.

The properties of charged black holes in string theory can be revealed by studying the geodesics around these solutions. This is because, except the information we get solving the classical equations of motion in the form of Einstein equations, we also get information about stringy corrections due to the string coupling which is of the order of the Planck scale. The study of null geodesics in the electrically charged GHS black hole was carried out in Refs. [13,14], and the timelike geodesics were analyzed in Refs. [14–18]. Additionally, in Ref. [19], the gravitational Rutherford scattering and Keplerian orbits were studied in the GHS black hole background, and the motion of massive particles with electric and magnetic charges in the background of a magnetically charged GHS stringy black hole were studied in Ref. [20].

The aim of this work is to consider the linear dilaton black hole solution [8] and to study the geodesic structure. Also, the aim is to analyze, via the Bañados, Silk, and West (BSW) mechanism, the possibility of obtaining unbounded energy in the center of mass frame of two colliding particles. Two particles colliding near the degenerate horizon of an extreme Kerr black hole could create a large c.m. energy if one of the particles has a critical angular momentum; thus, extreme Kerr black holes can act as natural particle accelerators, which is known as the BSW mechanism [21]. Then, based on an infinite acceleration being able to occur not only for extremal black holes but also for nonextremal ones [22], it is shown that infinite energy in the c.m. frame of colliding particles is a universal property of rotating black holes as long as the angular momentum of one of the colliding particles approaches the critical value [23]. However, it is shown that the similar effect exists for nonrotating charged black holes [24]. Also, the combination of the two mechanisms, the BSW effect and its analog for the collision of charged particles in the field of nonrotating charged black holes, has been studied in Ref. [25]. Moreover, the extension of the BSW mechanism to nonextremal backgrounds shows that particles cannot collide with arbitrarily high energies at the outer horizon and that ultraenergetic collisions can only occur near the Cauchy horizon of a Kerr black hole with any spin parameter [26]. The nonextremal Kerr-de Sitter black holes could also act as particle accelerators with arbitrarily high c.m. energy if one of the colliding particles has the critical angular momentum [27]. Also, it is known that two particles in the ergosphere lead to infinity growth of the energy of the c.m. frame, provided the angular momentum of one of the two particles has a large negative angular momentum and a fixed energy at infinity for the Kerr black holes [22], which was subsequently proven to be a universal property of the ergosphere [28]. The BSW mechanism has been studied for different black hole geometries. Higher-dimensional black holes have been studied, for instance, in Refs. [29–31], lower-dimensional black holes have been studied in Refs. [32–37], and stringy black holes have been studied in Ref. [38].

The manuscript is organized as follows. In Sec. II, we give a brief review of the linear dilaton black hole. Then, we obtain the equations of motion in Sec. III. In Sec. IV, we analyze the geodesics in the equatorial plane. In Sec. V, we obtain the c.m. energy of two colliding particles, we study the radial motion of a particle with critical angular momentum, and we investigate the possibility that the black hole acts as a particle accelerator. Then, in Sec. VI, we study the geodesics in four dimensions. Finally, our conclusions are in Sec. VII.

II. STATIC LINEAR DILATON BLACK HOLES

In this section, we will review how the linear dilaton black hole is extracted from the GHS solution [2]. The most general action of low energy heterotic string theory is given by

$$\mathcal{S}=\int d^{D}x\sqrt{-g}e^{-2\varphi}\Big[\Lambda+R+4(\nabla\varphi)^{2}-F_{\mu\nu}F^{\mu\nu}-\frac{1}{12}H_{\mu\nu\rho}H^{\mu\nu\rho}\Big], \tag{1}$$

where the scalar field φ is the dilaton field, $F_{\mu\nu}$ is a Maxwell field, and the 3-form $H_{\mu\nu\rho}$ is related to a 2-form potential $B_{\mu\nu}$ and the gauge field A_{μ} by $H=dB-A\wedge F$ so that $dH=-F\wedge F$. Note that in this action the term e^{φ} plays the role of a coupling constant giving the strength of the stringy effects.

If we set H to zero and make the conformal transformation of the metric to rescale $g_{\mu\nu}$ by $e^{-2\varphi}$ to get a metric with the standard Einstein action,

$$g^{E}_{\mu\nu}=e^{-2\varphi}g_{\mu\nu}. \tag{2}$$

The action now becomes (with $\Lambda=0$)

$$\mathcal{S}=\int d^4x\sqrt{-g_E}(R_E-2(\nabla\varphi)^2-e^{-2\varphi}F^2). \tag{3}$$

Rescaling the Einstein metric, we get a simple form of an electrically charged black hole,

$$ds_E^2=-\left(1-\frac{2M}{r}\right)dt^2+\left(1-\frac{2M}{r}\right)^{-1}dr^2 + r\left(r-\frac{Q^2}{M}\right)d\Omega, \tag{4}$$

$$F_{rt}=\frac{Q}{r^2},\qquad e^{2\phi}=1-\frac{Q^2}{Mr}. \tag{5}$$

Note that the metric in the r–t plane is identical to Schwarzschild. The only difference is that the area of the spheres is smaller. In fact, this area goes to zero when $r=Q^2/M$, and this surface is singular. Since g_{tt} remains finite at the singularity, there is no "infinite stretching" analogous to what happens to an observer hitting the singularity in Schwarzschild. As you increase Q, the singularity moves out in r. In the extremal limit $Q^2=2M^2$, the singularity coincides with the horizon. If you increase Q further, the singularity moves outside the horizon and becomes timelike.

Using these properties of the electrically charged GHS black hole, studying its near-horizon and near-extremal limits and the results of Ref. [39], a linear dilaton black hole solution was constructed in Ref. [8],

$$ds^2=\frac{r-b}{r_0}dt^2-\frac{r_0}{r-b}dr^2-r_0rd\Omega^2, \tag{6}$$

$$e^{2\phi}=\frac{r}{r_0},\qquad F_{tr}=\frac{1}{\sqrt{2}r_0}. \tag{7}$$

The two parameters r_0 and b have different physical meanings. The first describes the electric charge Q of the solution, which is given by the flux through a 2-sphere,

$$Q=\frac{1}{4\pi}\int e^{-2\phi}F^{0r}\sqrt{g}d\Omega=\frac{r_0}{\sqrt{2}}, \tag{8}$$

and characterizes the linear dilaton background, and the parameter b characterizing the black hole solution is proportional to its mass. This solution corresponds to the Schwarzschild black hole. However, the spacetime is not asymptotically flat.

Finally, this static lineal dilaton solution was generalized to a stationary one [8]:

$$ds^2=\frac{r^2-2Mr+a^2}{r_0r}dt^2-r_0r\left[\frac{dr^2}{r^2-2Mr+a^2}+d\theta^2 + \sin^2\theta\left(d\varphi-\frac{a}{r_0r}dt\right)^2\right], \tag{9}$$

$$F=\frac{1}{\sqrt{2}}\left[\frac{r^2-a^2\cos^2\theta}{r_0r^2}dr\wedge dt + a\sin 2\theta d\theta\wedge\left(d\varphi-\frac{a}{r_0r}dt\right)\right], \tag{10}$$

$$e^{-2\phi}=\frac{r_0r}{r^2+a^2\cos^2\theta}. \tag{11}$$

The Maxwell 2-form is derivable from the following 4-potential,

$$A=\frac{1}{\sqrt{2}}\left(\frac{r^2+a^2\cos^2\theta}{r_0r}dt+a\sin^2\theta d\varphi\right), \tag{12}$$

where the gauge is chosen such that the vector magnetic potential is regular on the axis $\theta=0$.

Although the metric (9) was derived from the Kerr metric, it differs in its asymptotic behavior ($r\to\infty$), which is the same as for the linear dilaton metric and in its behaviour near $r=0$. In the case of the Kerr metric, $r=0$ is the equation of a disk through which the metric can be continued to negative r, while in (9), $r=0$ is a timelike line singularity. Also, the Penrose diagrams of (9) for the three cases $M^2>a^2$, $M^2=a^2$, and $M^2<a^2$ are not identical to those of the Kerr spacetime, but rather to those of the Reissner-Nordström spacetime, with the charge replaced by the angular-momentum parameter a.

III. MOTION EQUATIONS OF PARTICLES IN A LINEAR DILATON BLACK HOLE

Now, in order to obtain the motion equations of particles and photons in a linear dilaton black hole, we rewrite the metric (9) as

$$ds^2=-f(r)dt^2+\frac{dr^2}{f(r)} + h(r)\left(d\theta^2+\sin^2\theta\left(d\varphi-a\frac{dt}{h(r)}\right)^2\right), \tag{13}$$

where

$$f(r)=\frac{r^2-2Mr+a^2}{r_0r}=\frac{(r-r_+)(r-r_-)}{r_0r},\qquad h(r)=r_0r \tag{14}$$

and r_0 is a positive constant. The outer and inner horizons are given by

$$r_{\pm} = M \pm \sqrt{M^2 - a^2}. \tag{15}$$

It is worth noting that the geodesic structure of the linear dilaton black hole was studied in Ref. [40] for the nonrotating case. Here, we shall extend such a study by considering the rotating case.

So, we first derive the equations of motion following the same approach given in Ref. [41]. We consider the motion of test particles with mass m and photons. Thus, in order to obtain the equation of motion, we apply the Hamilton-Jacobi formalism. In this sense, the Hamilton-Jacobi equation for the geometry described by the metric $g_{\mu\nu}$ is

$$2\frac{\partial S}{\partial \tau} = g^{\mu\nu}\frac{\partial S}{\partial x^{\mu}}\frac{\partial S}{\partial x^{\nu}}. \tag{16}$$

So, in order to solve the Hamilton-Jacobi equation, and taking into account the symmetries of the metric, we use the following ansatz for the action,

$$S = -\frac{1}{2}m^2\tau - Et + S_r(r) + S_{\theta}(\theta) + L\varphi, \tag{17}$$

where E and L are identified as the energy and angular momentum of the particle. Thus, replacing this ansatz in Eq. (16) yields

$$\left(\frac{\partial S_r}{\partial r}\right)^2 - \left(\frac{E}{f(r)} - \frac{aL}{h(r)f(r)}\right)^2 + \frac{m^2}{f(r)} + \frac{1}{h(r)f(r)}\left(\left(\frac{\partial S_{\theta}}{\partial \theta}\right)^2 + \frac{L^2}{\sin^2\theta}\right) = 0. \tag{18}$$

Now, using the standard procedure, we recognize the following constant,

$$k^2 = \left(\frac{\partial S_{\theta}}{\partial \theta}\right)^2 + \frac{L^2}{\sin^2\theta}, \tag{19}$$

which is identified as the Carter separability constant. Then, we obtain the following equation for the radial component of the action:

$$\left(\frac{\partial S_r}{\partial r}\right)^2 - \left(\frac{E}{f(r)} - \frac{aL}{h(r)f(r)}\right)^2 + \frac{k^2 + m^2h(r)}{h(r)f(r)} = 0. \tag{20}$$

Thus, the formal solutions for the radial and polar components of the action are given by

$$S_r(r, k^2, E, L) = \epsilon\int\sqrt{\left(E - \frac{aL}{r_0 r}\right)^2 - f(r)\left(m^2 + \frac{k^2}{r_0 r}\right)}\frac{dr}{f(r)}, \tag{21}$$

$$S_{\theta}(\theta, k^2, L) = \epsilon\int\sqrt{k^2 - \frac{L^2}{\sin^2\theta}}d\theta, \tag{22}$$

where $\epsilon = \pm 1$. Now, using the Hamilton-Jacobi method and making $\frac{\delta S}{\delta k^2} = 0$, $\frac{\delta S}{\delta m^2} = 0$, $\frac{\delta S}{\delta E} = 0$, and $\frac{\delta S}{\delta L} = 0$, we simplify our study to the following quadrature problem:

$$\int\frac{d\theta}{\sqrt{k^2 - \frac{L^2}{\sin^2\theta}}} = \int\frac{dr}{r_0 r\sqrt{(E - \frac{aL}{r_0 r})^2 - f(r)(m^2 + \frac{k^2}{r_0 r})}}, \tag{23}$$

$$\tau(r) = \epsilon\int\frac{dr}{\sqrt{(E - \frac{aL}{r_0 r})^2 - f(r)(m^2 + \frac{k^2}{r_0 r})}}, \tag{24}$$

$$t(r) = \epsilon\int\frac{(E - \frac{aL}{r_0 r})dr}{f(r)\sqrt{(E - \frac{aL}{r_0 r})^2 - f(r)(m^2 + \frac{k^2}{r_0 r})}}, \tag{25}$$

$$\varphi(r) = \epsilon\int\frac{(E - \frac{aL}{r_0 r})\frac{a}{r_0 r}}{\sqrt{(E - \frac{aL}{r_0 r})^2 - f(r)(m^2 + \frac{k^2}{r_0 r})}}\frac{dr}{f(r)} + \epsilon\int\frac{L}{\sin^2\theta\sqrt{k^2 - \frac{L^2}{\sin^2\theta}}}d\theta. \tag{26}$$

Then, by defining the Mino time γ as $d\gamma = d\tau/(r_0 r)$, we can write the equations of motion in terms of the new time parameter, which yields

$$\left(\frac{d\theta}{d\gamma}\right)^2 = k^2 - \frac{L^2}{\sin^2\theta}, \tag{27}$$

$$\left(\frac{dr}{d\gamma}\right)^2 = r_0^2 r^2\left(\left(E - \frac{aL}{r_0 r}\right)^2 - f(r)\left(m^2 + \frac{k^2}{r_0 r}\right)\right), \tag{28}$$

$$\frac{d\varphi}{d\gamma} = \left(E - \frac{aL}{r_0 r}\right)\frac{a}{f(r)} + \frac{L}{\sin^2\theta}, \tag{29}$$

$$\frac{dt}{d\gamma} = \frac{r_0 r(E - \frac{aL}{r_0 r})}{f(r)}. \tag{30}$$

In this way, we have the equations of motion for our particles moving in the background of the linear dilaton black hole. In the next section, we will perform an analysis of the equations of motion in the equatorial plane.

IV. GEODESICS IN THE EQUATORIAL PLANE

The Lagrangian associated with the motion in the equatorial plane, that is, $\theta = \pi/2$ and $\dot{\theta} = 0$, turns out to be

$$2\mathcal{L} = -\frac{r^2 - 2Mr}{r_0 r}\dot{t}^2 - 2a\dot{t}\dot{\phi} + \frac{r_0 r}{r^2 - 2Mr + a^2}\dot{r}^2 + r_0 r\dot{\phi}^2, \tag{31}$$

where $\dot{q} = dq/d\tau$ and τ is an affine parameter along the geodesic that we choose as the proper time. Since the Lagrangian (31) is independent of the cyclic coordinates (t, ϕ), then their conjugate momenta (Π_t, Π_ϕ) are conserved. Then, the equations of motion are obtained from $\dot{\Pi}_q - \frac{\partial \mathcal{L}}{\partial q} = 0$ and yield

$$\dot{\Pi}_t = 0, \quad \dot{\Pi}_r = -\frac{\dot{t}^2}{2r_0} - \frac{r_0(r^2-a^2)\dot{r}^2}{2(r^2-2Mr+a^2)^2} + \frac{r_0\dot{\phi}^2}{2} \quad \text{and}$$
$$\dot{\Pi}_\phi = 0, \tag{32}$$

where $\Pi_q = \partial\mathcal{L}/\partial\dot{q}$ are the conjugate momenta to the coordinate q and are given by

$$\begin{aligned}\Pi_t &= -\frac{r^2-2Mr}{r_0 r}\dot{t} - a\dot{\phi} \equiv -E,\\ \Pi_r &= \frac{r_0 r}{r^2-2Mr+a^2}\dot{r} \quad \text{and}\\ \Pi_\phi &= -a\dot{t} + r_0 r\dot{\phi} \equiv L,\end{aligned} \tag{33}$$

where E and L are dimensionless integration constants associated to each of them. Therefore, the Hamiltonian is given by

$$\mathcal{H} = \Pi_t\dot{t} + \Pi_\phi\dot{\phi} + \Pi_r\dot{r} - \mathcal{L} \tag{34}$$

$$2\mathcal{H} = -E\dot{t} + L\dot{\phi} + \frac{r_0 r}{r^2-2Mr+a^2}\dot{r} \equiv -m^2. \tag{35}$$

Now, by normalization, we shall consider that $m^2 = 1$ for massive particles and $m^2 = 0$ for photons. Therefore, we obtain

$$\dot{\phi} = \frac{r_0 r a E + (r^2-2Mr)L}{r_0 r(r^2-2Mr+a^2)}, \tag{36}$$

$$\dot{t} = \frac{r_0 r E - aL}{r^2-2Mr+a^2}, \tag{37}$$

$$\begin{aligned}\dot{r}^2 &= \left(E - \frac{aL}{r_0 r}\right)^2 - \frac{r^2-2Mr+a^2}{r_0 r}\left(m^2 + \frac{L^2}{r_0 r}\right)\\ &= (E-V_-)(E-V_+),\end{aligned} \tag{38}$$

where $V_\pm(r)$ is the effective potential and it is given by

$$V_\pm(r) = \frac{aL}{r_0 r} \pm \sqrt{\frac{r^2-2Mr+a^2}{r_0 r}\left(m^2 + \frac{L^2}{r_0 r}\right)}. \tag{39}$$

Since the negative branch has no classical interpretation, it is associated with antiparticles in the framework of quantum field theory [42], and we choose the positive branch of the effective potential $V = V_+$. In the next section, we will perform a general analysis of the equations of motion.

In linear dilaton black hole, the presence of $g_{t\phi} \neq 0$ in the metric introduces qualitatively new effects on particle and photon trajectories, like the effect called "dragging of inertial frames." Thus, by using Eqs. (36) and (37), we obtain

$$\dot{\phi}/\dot{t} = \frac{d\phi}{dt} = \frac{r_0 a E + (r-2M)L}{r_0(r_0 r E - aL)} \equiv \omega(r). \tag{40}$$

This equation defines $\omega(r)$, the angular velocity of the test particle. Notice that if we consider a zero angular-momentum particle ($L = 0$) the angular velocity of the test particle is given by

$$\omega(r) = \frac{a}{r_0 r}. \tag{41}$$

So, a remarkable result is that a particle dropped "straight in" ($L = 0$) from a finite distance is "dragged" just by the influence of gravity. Therefore, the test particle acquires an angular velocity (ω), with the same sign as a. Also, this effect weakens with distance as $1/r$. It is worth mentioning that for the Kerr metric this effect weakens with the distance as $1/r^3$ [43].

Following a similar treatment given in Ref. [43] for the Kerr geometry, we consider photons emitted in the equatorial plane ($d\theta = 0$) at some given r. In particular, we consider those photons initially going in the $\pm\phi$-direction, that is tangent to a circle of constant r ($dr = 0$). Then, they generally have only dt and $d\phi$ nonzero on the path at first, and since $ds^2 = 0$, from the metric (2.9), we have

$$0 = g_{tt}dt^2 - 2a\sin^2\theta dt d\phi + r_0 r\sin^2\theta d\phi^2, \tag{42}$$

where

$$g_{tt} = \frac{r^2-2Mr+a^2\cos^2\theta}{r_0 r}. \tag{43}$$

Thus, Eq. (42) can be written as

$$0 = g_{tt} - 2a\sin^2\theta\omega + r_0 r\sin^2\theta\omega^2. \tag{44}$$

It is worth mentioning that a remarkable effect happens if $g_{tt} = 0$; the two solutions are given by

$$\omega_1 = 0 \ \text{ and } \ \omega_2 = \frac{2a}{r_0 r}. \tag{45}$$

Notice that the second solution, ω_2, gives the same sign as the parameter a, and it represents the photon sent off in the same direction as the rotating black hole. The other solution, ω_1, means that the other photon, the one sent backward initially, does not move at all. The dragging of orbits has become so strong that this photon cannot move in the direction opposite to the rotation. The surface where

$g_{tt} = 0$ is called the ergosphere or "static limit," since inside it no particle can remain at fixed r, θ, ϕ, and this occurs at

$$r_e = M + \sqrt{M^2 - a^2 \cos^2\theta}, \tag{46}$$

with r_e the radius of the ergosphere, which lies outside the horizon (15) and coincides with the event horizon only at the poles $\theta = 0$ and $\theta = \pi$. Inside this radius, since $g_{tt} > 0$, all particles and photons must rotate with the black hole. This result is similar to the Kerr metric [43].

On the other hand, as in the Kerr solution, in the linear dilaton black hole, the ergosphere occurs at $g_{tt} = 0$, and the horizon is at $g_{rr} = 0$. The horizon r_+ is a surface of constant r and t, and any surface of constant r and t has an intrinsic metric of which the line element comes from Eq. (2.9) with $dt = dr = 0$:

$$ds^2 = r_0 r_+ d\theta^2 + r_0 r_+ \sin^2\theta d\phi^2. \tag{47}$$

The proper area of this surface, $\mathcal{A}$, is given by integrating the square root of the determinant of this metric over all θ and ϕ,

$$\mathcal{A} = \int_0^{2\pi}\int_0^{\pi} r_0 r_+ \sin\theta d\theta d\phi = 4\pi r_0 r_+, \tag{48}$$

which is different than the result for the Kerr geometry [43].

A. Timelike geodesics

In this case ($m = 1$), for timelike geodesics, the effective potential is given by

$$V(r) = \frac{aL}{r_0 r} + \sqrt{\frac{r^2 - 2Mr + a^2}{r_0 r}\left(1 + \frac{L^2}{r_0 r}\right)}, \tag{49}$$

the behaviors of which are given in Fig. 1 for particles with $a > 0$ (direct geodesics) and $a < 0$ (retrograde geodesics), where E corresponds to the energy of the particle, the trajectory of which is allowed for direct and retrograde geodesics, $E_1 = V(r_+, |a|)$ and $E_2 = V(r_+, -|a|)$. Notice that retrograde geodesics allow trajectories with negative energy with $E > E_2$. However, the behavior of the trajectories are similar in both cases, being bounded orbits with a finite return point R_i, which is given by

$$R_i = \frac{r_0^2E^2 + 2Mr_0 - L^2}{2r_0} \times \left(1 + \sqrt{1 + \frac{4r_0(2ML^2 - 2aELr_0 - r_0a^2)}{(r_0^2E^2 + 2Mr_0 - L^2)^2}}\right). \tag{50}$$

This return point for a given energy E is greater for retrograde geodesics than for direct geodesics. Now, in order to obtain the solution for the proper time, we integrate Eq. (36), and we obtain

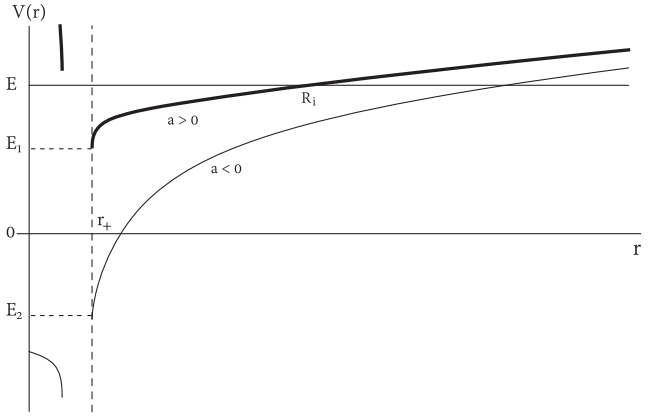

FIG. 1. The behavior of the effective potential for massive particles as a function of r, $r_0 = 1$, $M = 2$, $L = 4$, and $|a| = 1.9$.

$$\tau(r) = \frac{r_0(F(r) - F(R_i))}{4\sqrt{2ML^2 - 2aELr_0 - r_0a^2}}, \tag{51}$$

where

$$F(r) = \frac{2\zeta(\Omega)\wp^{-1}[U(r)]}{\wp'(\Omega)} + \frac{1}{\wp'(\Omega)}\ln\left|\frac{\sigma[\wp^{-1}[U(r)] - \Omega]}{\sigma[\wp^{-1}[U(r)] + \Omega]}\right|, \tag{52}$$

with $\wp^{-1}(Y) \equiv \wp^{-1}(Y; g_2, g_3)$ being the inverse P-Weierstrass function, $\sigma(Y) \equiv \sigma(Y; g_2, g_3)$ being the sigma Weierstrass function, $\zeta(Y) \equiv \zeta(Y; g_2, g_3)$ being the zeta Weierstrass function, and the Weierstrass invariants given by

$$g_2 = \frac{1}{12}\left(\frac{r_0^2E^2 + 2Mr_0 - L^2}{2ML^2 - 2aELr_0 - r_0a^2}\right)^2 + \frac{1}{4}\left(\frac{r_0}{2ML^2 - 2aELr_0 - r_0a^2}\right) \tag{53}$$

and

$$g_3 = \frac{-1}{216}\left(\frac{r_0^2E^2 + 2Mr_0 - L^2}{2ML^2 - 2aELr_0 - r_0a^2}\right)^3 - \frac{1}{48}\frac{r_0(r_0^2E^2 + 2Mr_0 - L^2)}{(2ML^2 - 2aELr_0 - r_0a^2)^2}. \tag{54}$$

Also, the radial function $U = U(r)$ and the constant Ω are given by

$$U(r) = \frac{1}{4r} + \frac{1}{12}\left(\frac{r_0^2E^2 + 2Mr_0 - L^2}{2ML^2 - 2aELr_0 - r_0a^2}\right) \tag{55}$$

and

$$\Omega = \wp^{-1}\left(\frac{1}{12}\left(\frac{r_0^2E^2 + 2Mr_0 - L^2}{2ML^2 - 2aELr_0 - r_0a^2}\right)\right). \tag{56}$$

Now, we consider the solution of the trajectory in the coordinate time in order to compare both times,

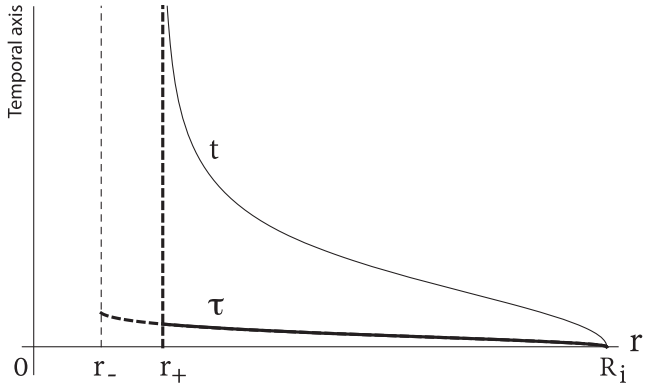

FIG. 2. The behavior of the proper (τ) and coordinate (t) times for ingoing particles ($L > 0$) as function of r, with $M = 2$, $a = 1$, 9, $L = 4$, and $r_0 = 1$.

$$t(r) = -A_+[F_+(r) - F_+(R_i)] + A_-[F_-(r) - F_-(R_i)], \tag{57}$$

where

$$F_\pm(r) = \frac{2\zeta(\Omega_\pm)\wp^{-1}[U(r)]}{\wp'(\Omega_\pm)} + \frac{1}{\wp'(\Omega_\pm)}\ln\left|\frac{\sigma[\wp^{-1}[U(r)] - \Omega_\pm]}{\sigma[\wp^{-1}[U(r)] + \Omega_\pm]}\right|, \tag{58}$$

$$\Omega_\pm = \wp^{-1}\left[\frac{1}{12}\left(\frac{r_0^2E^2 + 2Mr_0 - L^2}{2ML^2 - 2aELr_0 - r_0a^2}\right) + \frac{1}{4r_\pm}\right], \tag{59}$$

$$A_\pm = \frac{r_0(r_0E - aLr_\pm)}{4(r_+ - r_-)\sqrt{2ML^2 - 2aELr_0 - r_0a^2}}. \tag{60}$$

Then, in Fig. 2, we plot the proper (τ) and coordinate (t) times as a function of r for a particle falling from a finite distance with zero initial velocity; we can see that the particle falls toward the horizon in a finite proper time. The situation is very different if we consider the trajectory in the coordinate time, where t goes to infinity. This physical result is consistent with the Kerr black hole.

The solution for $\phi(r)$ is given by

$$\phi(r) = -B_+[F_+(r) - F_+(R_i)] + B_-[F_-(r) - F_-(R_i)] \tag{61}$$

with

$$B_\pm = \frac{L + r_\pm(r_0aE - 2ML)}{4(r_+ - r_-)\sqrt{2ML^2 - 2aELr_0 - r_0a^2}}. \tag{62}$$

In Fig. 3, we plot the behavior of $\phi(r)$, and we can observe that a trajectory approaching the horizon will spiral around the black hole an infinite number of times such as was observed by Chandrasekhar for the geodesics in the Kerr spacetime [41].

1. Radial geodesics

In this case ($L = 0$), the effective potential reads

$$V(r) = \sqrt{\frac{r^2 - 2Mr + a^2}{r_0r}}. \tag{63}$$

Notice that the effective potential is the same for direct and retrograde geodesics. The behavior of the effective potential for massive particles is plotted in Fig 4. The turning point, R_F, can be obtained from Eq. (50) by imposing $L = 0$ and is given by

$$R_F = \frac{r_0E^2 + 2M}{2}\left(1 + \sqrt{1 - \frac{4a^2}{(r_0E^2 + 2M)^2}}\right), \tag{64}$$

It is worth mentioning that the radial motion allows only bounded orbits, which is similar to the trajectories with angular momentum. However, we can observe that the energy of a particle without angular momentum must be positive ($E > 0$) independently of whether it is a direct or a retrograde geodesics. In contrast, orbits with negative or null energy are possible for retrograde trajectories with angular momentum. On the other hand, the solutions for

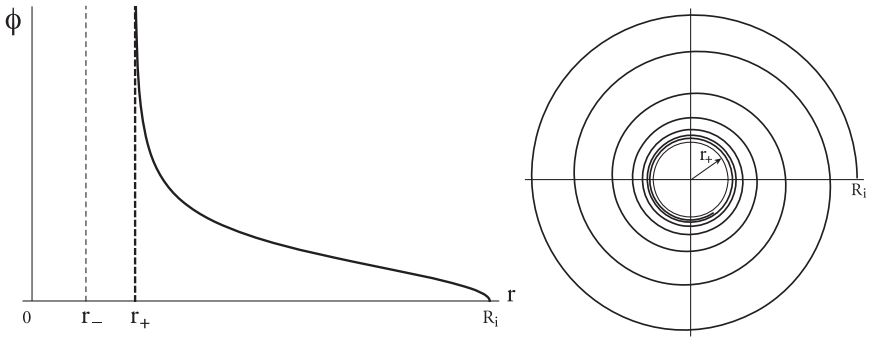

FIG. 3. The behavior of $\phi(r)$ for ingoing particles ($L > 0$), with $M = 2$, $a = 1$, 9, $L = 4$, and $r_0 = 1$.

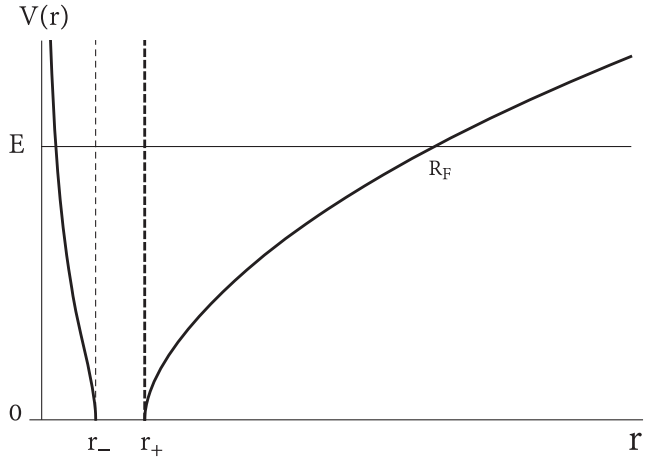

FIG. 4. The behavior of the effective potential for massive particles as a function of r, $r_0 = 1$, $M = 2$, $L = 4$, $|a| = 1.9$, $R_F = 10$, and $E = 2.52$.

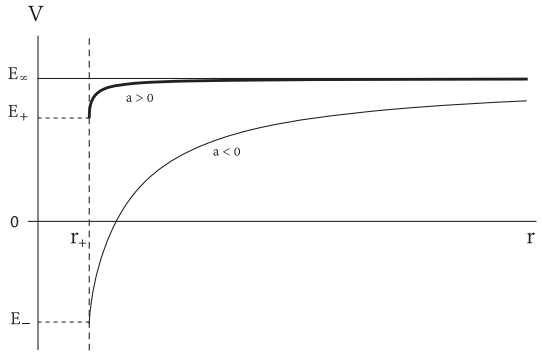

FIG. 5. The behavior of the effective potential for photons ($L > 0$) as a function of r, with $r_0 = 1$, $M = 2$, and $|a| = 1.9$.

$\phi(r)$, $\tau(r)$, and $t(r)$ have a behavior similar to that of particles with angular momentum due to the effective potential.

B. Null geodesics in the equatorial plane

In this section, we analyze the motion of photons, $m^2 = 0$; so, the effective potential is given by

$$V(r) = \frac{L}{r_0 r}\left(a + \sqrt{r^2 - 2Mr + a^2}\right), \tag{65}$$

the behavior of which is given in Fig. 5 for photons with $a > 0$ (direct null geodesics) and $a < 0$ (retrograde null geodesics), where $E_\infty = L/r_0$ corresponds to the energy of the photon when $r \to \infty$.$E_+ = V(r_+, |a|)$ and $E_- = V(r_+, -|a|)$. Notice that retrograde null geodesics allow trajectories with negative energy with $E > E_-$. However, in this case, we can distinguish two zones; one of them allows bounded orbits ($E < E_\infty$), and the other one allows unbounded orbits ($E \geq E_\infty$).

1. Direct null bounded trajectory

Now, we consider the direct null bounded trajectory, which is allowed for $E_+ < E < E_\infty$, and the return point of the photon yields

$$r_i = \frac{2L(ML - ar_0E)}{L^2 - r_0^2E^2}. \tag{66}$$

So, choosing the initial conditions for the photons as $r = r_i$ when $\phi = t = \tau = 0$, Eqs. (36) and (37) yield

$$\tau(r) = \frac{r_0}{\sqrt{L^2 - E^2r_0^2}}\left[\sqrt{r_i r - r^2} + r_i \tan^{-1}\sqrt{\frac{r_i}{r} - 1}\right], \tag{67}$$

$$\begin{aligned} t(r) = A_0 \Bigg[& 2\tan^{-1}\sqrt{\frac{r_i}{r} - 1} \\ & + A_1 \ln\left[\frac{\sqrt{r(r_i - r_+)} + \sqrt{r_+(r_i - r)}}{\sqrt{r(r_i - r_+)} - \sqrt{r_+(r_i - r)}}\right]\Bigg] \\ & + A_0A_2 \ln\left[\frac{\sqrt{r(r_i - r_-)} + \sqrt{r_-(r_i - r)}}{\sqrt{r(r_i - r_-)} - \sqrt{r_-(r_i - r)}}\right], \end{aligned} \tag{68}$$

where the constants A_0, A_1, and A_2 are given by

$$\begin{aligned} A_0 &= \frac{r_0^2 E}{\sqrt{L^2 - E^2r_0^2}}, \\ A_1 &= \frac{r_+(r_+ - aL/r_0E)}{(r_+ - r_-)\sqrt{r_+(r_i - r_+)}}, \\ A_2 &= \frac{r_-(aL/r_0E - r_-)}{(r_+ - r_-)\sqrt{r_-(r_i - r_-)}}, \end{aligned} \tag{69}$$

and Eq. (38) yields

$$\begin{aligned} \phi(r) = B_0 \Bigg[& 2\tan^{-1}\sqrt{\frac{r_i}{r} - 1} \\ & + B_1 \ln\left[\frac{\sqrt{r(r_i - r_+)} + \sqrt{r_+(r_i - r)}}{\sqrt{r(r_i - r_+)} - \sqrt{r_+(r_i - r)}}\right]\Bigg] \\ & + B_0B_2 \ln\left[\frac{\sqrt{r(r_i - r_-)} + \sqrt{r_-(r_i - r)}}{\sqrt{r(r_i - r_-)} - \sqrt{r_-(r_i - r)}}\right], \end{aligned} \tag{70}$$

and the constants B_0, B_1, and B_2 are given by

$$\begin{aligned} B_0 &= \frac{L}{\sqrt{L^2 - E^2r_0^2}}, \\ B_1 &= \frac{r_+(r_+ - 2M + ar_0E/L)}{(r_+ - r_-)\sqrt{r_+(r_i - r_+)}}, \\ B_2 &= \frac{r_-(2M - ar_0E/L - r_-)}{(r_+ - r_-)\sqrt{r_-(r_i - r_-)}}. \end{aligned} \tag{71}$$

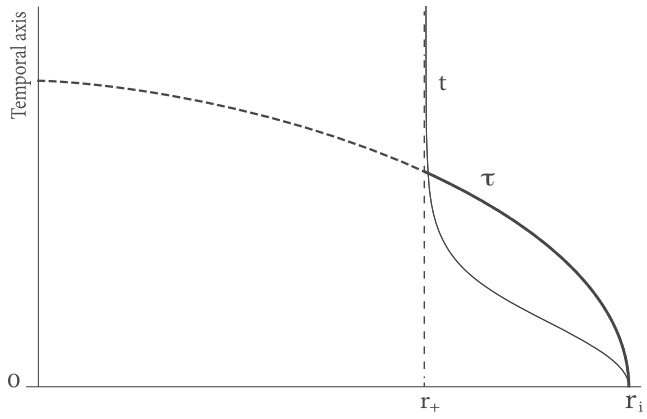

FIG. 6. The behavior of the proper (τ) and coordinate (t) times for ingoing photons ($L > 0$) as function of r, with $r_0 = 1$, $M = 2$, $r_i = 4$, and $a = 1.9$.

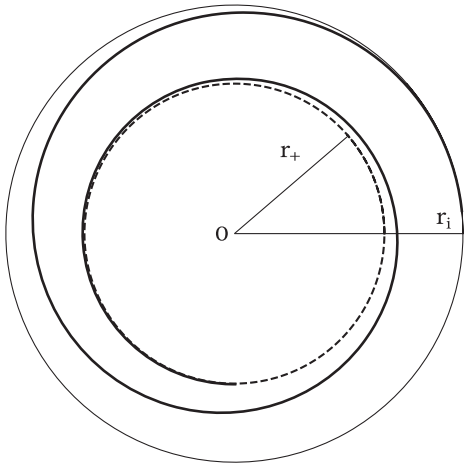

FIG. 7. The behavior of $\phi(r)$ for ingoing photons ($L > 0$), with $r_0 = 1$, $M = 2$, $r_i = 4$, and $a = 1.9$.

Then, in Fig. 6, we plot the proper (τ) and coordinate (t) times as a function of r for a photon falling from a finite distance; we can see that the photon falls toward the horizon in a finite proper time. The situation is very different if we consider the trajectory in the coordinate time, where t goes to infinity. Also, in Fig. 7, we plot the behavior of $\phi(r)$, and we can observe that a trajectory approaching the horizon will spiral around the black hole an infinite number of times.

2. Direct null unbounded trajectory

Photons with energy $E_\infty \leq E$ do not have a barrier of potential nor turning point. So, the photons can plunge into the horizon or escape to spatial infinity. In this section, we consider the special case $E = E_\infty = V(\infty) = L/r_0$ for simplicity. Thus, choosing the initial conditions for the photons $\phi = t = \tau = 0$, when $r = r_i$, Eqs. (36), (37), and (38) yield

$$\tau(r) = \pm\frac{2k_0}{3}[r^{3/2} - r_i^{3/2}], \quad \text{and} \quad k_0 = \frac{r_0}{L\sqrt{2(M-a)}}, \tag{72}$$

$$t(r) = \pm\frac{k_0 L}{(r_+ - r_-)}[(r_+ - a)[T_+(r) - T_+(r_i)] + (a - r_-)[T_-(r) - T_-(r_i)]], \tag{73}$$

and

$$\phi(r) = \pm\frac{k_0 L}{r_0(r_+ - r_-)}[(r_+ - 2M + a)[T_+(r) - T_+(r_i)] + (2M - a - r_-)[T_-(r) - T_-(r_i)]], \tag{74}$$

where

$$T_\pm(r) = 2\sqrt{r} - 2\sqrt{r_\pm}\tanh^{-1}\sqrt{\frac{r}{r_\pm}}. \tag{75}$$

The plus and minus signs correspond to trajectories that escape to infinity or that plunge into the horizon, respectively. In Sec. V, we will plot the unbounded trajectories for photons. Notice that from Eq. (72) in the proper frame the photons arrive at the event horizon in a finite proper time.

3. Radial motion

Radial motion corresponds to a trajectory with null angular momentum $L = 0$, and photons are destined to fall toward the event horizon. From Eq. (39), we can see that for radial photons we have $V(r) = 0$, so Eqs. (37), (38), and (36) in the equatorial plane become

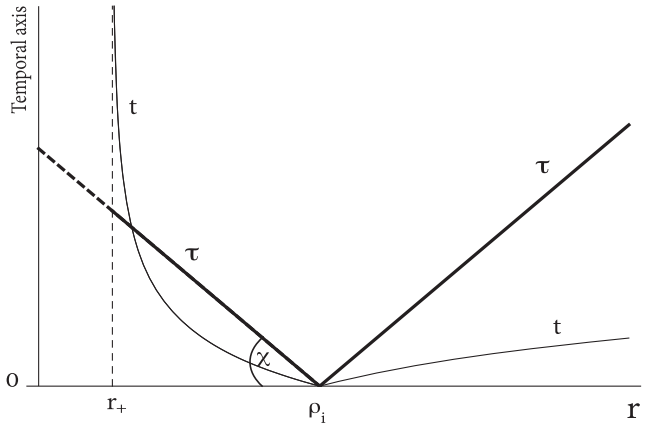

FIG. 8. The variation of the coordinate (t) and the proper (τ) times along an unbounded timelike radial geodesic described by a photon as a test particle, starting at $\rho_i = 10$ and falling toward the singularity or going toward infinity, for $M = 2$, $a = 1$, 9, and $r_0 = 1$, where $\chi = \tan^{-1}(1/E)$. The thick line is for the proper time, and thin line is for the coordinate time. The dashed part of the curve inside the horizon has no physical meaning.

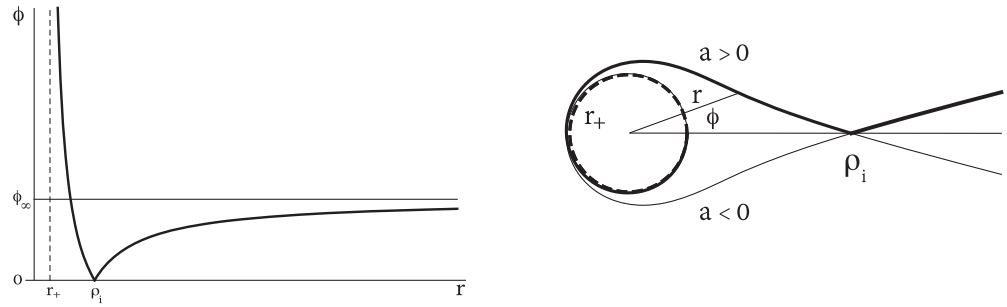

FIG. 9. The behavior for $\phi(r)$ for the direct and retrograde trajectory starting at $\rho_i = 10$ and falling toward the singularity or going toward infinity, for $M = 2$, $a = 1$, 9, and $r_0 = 1$.

$$\dot{t} = \frac{r_0 r E}{r^2 - 2Mr + a^2}, \tag{76}$$

$$\dot{\phi} = \frac{aE}{(r^2 - 2Mr + a^2)}, \tag{77}$$

$$\pm\dot{r} = E, \tag{78}$$

where the sign $(-)$ corresponds to photons falling into the event horizon and the sign $(+)$ corresponds to photons that escape to infinity. Choosing the initial conditions for the photons as $r = \rho_i$ when $\phi = t = \tau = 0$, Eq. (78) yields

$$\tau(r) = \pm\frac{1}{E}(r - \rho_i), \tag{79}$$

where the sign $\pm$ has the same meaning as given previously. Note that the above equation depends on the energy E, and it is valid for retrograde and direct geodesics. Also, for the negative sign, the photons, in the proper frame, arrive at the event horizon in a finite proper time; see Fig. 8. On the other hand, a straightforward integration of Eqs. (76) and (77) leads to

$$t(r) = \pm\frac{r_0}{r_+ - r_-}\left[r_+ \ln\left|\frac{r - r_+}{\rho_i - r_+}\right| - r_- \ln\left|\frac{r - r_-}{\rho_i - r_-}\right|\right] \tag{80}$$

and

$$\phi(r) = \pm\frac{a}{r_+ - r_-}\left[\ln\left|\frac{r - r_+}{\rho_i - r_+}\right| - \ln\left|\frac{r - r_-}{\rho_i - r_-}\right|\right]. \tag{81}$$

Note that the solution for the coordinate time t does not depend on the energy of the photon and the expression is valid for retrograde and direct geodesics. While the solution for ϕ does not depend on the energy of the photon either, but it depends on the angular-momentum parameter a, see Fig. 9. Moreover, for a direct geodesic when $r \to \infty$,

$$\phi_\infty = \frac{a}{r_+ - r_-}\ln\left|\frac{\rho_i - r_-}{\rho_i - r_+}\right|. \tag{82}$$

It is worth mentioning that another remarkable feature of the motion of photons is the existence of circular orbits of any radius. This occurs in the extremal case $(M = a)$ and for $L = Er_0$.

V. THE C.M. ENERGY OF TWO COLLIDING PARTICLES

In this section, we study the c.m. energy of two colliding massive particles in the equatorial plane $\theta = \pi/2$, and the 4-velocity of the test particles is given by $u = (\dot{t}, \dot{r}, 0, \dot{\phi})$, where

$$\dot{t} = \frac{r_0 r E - aL}{r_0 r f(r)}, \tag{83}$$

$$\dot{r}^2 = \left(E - \frac{aL}{r_0 r}\right)^2 - f(r)\left(1 + \frac{L^2}{r_0 r}\right), \tag{84}$$

$$\dot{\phi} = \frac{aEr_0 r + Lr_0 r f(r) - a^2 L}{r_0^2 r^2 f(r)}. \tag{85}$$

We will assume that $\dot{t} > 0$ for all $r > r_+$ so that the motion is forward in time outside the horizon, so

$$r_0 r E - aL > 0, \quad \text{for all } r > r_+. \tag{86}$$

Now, we use the 4-velocity components to obtain the c.m. energy of the collision of two particles in the linear dilaton black hole, and we consider that the particles have energies E_1 and E_2 and angular momenta L_1 and L_2, respectively. Thus, using the relation $E_{\text{c.m.}} = \sqrt{2}m_0\sqrt{1 - g_{\mu\nu}u_1^\mu u_2^\nu}$, where m_0 denotes the rest mass of the particles and u_1 and u_2 denote the 4-velocities of the particles, we obtain

$$\frac{E_{\text{c.m.}}^2}{2m_0^2} = \frac{r_0 r f(r)(r_0 r - L_1 L_2) + (K_1 K_2 - H_1 H_2)}{r_0^2 r^2 f(r)}, \tag{87}$$

where

$$K_i = E_i r_0 r - aL_i,$$
$$H_i = \sqrt{(E_i r_0 r - aL_i)^2 - r_0 r f(r)(r_0 r + L_i^2)}, \tag{88}$$

with $i = 1, 2$. When the particles arrive at the horizon $r = r_+$, $f(r) \to 0$, $H_1 \to \sqrt{K_1^2}$, and $H_2 \to \sqrt{K_2^2}$; therefore,

$$\frac{E^2_{\text{c.m.}}}{2m_0^2}(r \to r_+) = \frac{1}{r_0^2 r^2 f(r)}\left(K_1K_2 - \sqrt{K_1^2}\sqrt{K_2^2}\right). \tag{89}$$

Notice that for $K_1K_2 < 0$ the $E_{\text{c.m.}}$ on the horizon ($f(r) = 0$) is negative infinite, which is not a physical solution. However, when $K_1K_2 > 0$, the numerator of this expression will be zero, and the value of $E_{\text{c.m.}}$ will be undetermined. In order to obtain the limiting value, we use the l'Hôpital rule and obtain

$$\frac{E^2_{\text{c.m.}}}{2m_0} = \frac{r_0 r_+ (K_1(r_+) + K_2(r_+))^2 + (K_1(r_+)L_2 - K_2(r_+)L_1)^2}{2r_0 r_+ K_1(r_+)K_2(r_+)}. \tag{90}$$

Note that the numerator of the above expression is finite at the horizon and when $K_i(r_+) = 0$ the c.m. energy of two colliding particles on the horizon could be arbitrarily high, $E_{\text{c.m.}}|_{K_i=0} \to \infty$. From $K_i(r_+) = 0$, we obtain the critical angular momentum:

$$L_{ci} = \frac{r_0 r_+ E_i}{a}, \quad i = 1, 2. \tag{91}$$

Besides, when $K_1(r_+)$ and $K_2(r_+)$ are both zero, then $E_{\text{c.m.}}$ is finite. In this case, $H_1(r_+) = H_2(r_+) = 0$, and

$$\frac{E^2_{\text{c.m.}}}{2m_0} = 1 - \frac{L_1L_2}{r_0 r_+}. \tag{92}$$

Therefore, in order to obtain infinite c.m. energy, only one of the colliding particles must have the critical angular momentum.

By a similar analysis, it is possible to evaluate the $E_{\text{c.m.}}$ on the inner horizon, finding that this is also infinite as long as one of the two particles has the following critical angular momentum:

$$L_{ci} = \frac{r_0 r_- E_i}{a}, \qquad i = 1, 2. \tag{93}$$

Now, in order to see if a particle with critical angular momentum could reach the horizon, we shall analyze the radial motion of the particle with critical angular momentum and energy E, and we shall find the region where it can exist. The radial equation can be written as

$$\dot{r}^2 = R(r), \tag{94}$$

where

$$\begin{aligned} R(r) &= \left(E - \frac{aL}{r_0 r}\right)^2 - f(r)\left(1 + \frac{L^2}{r_0 r}\right) \\ &= -\frac{r}{r_0} + \frac{2ML^2 - r_0a^2 - 2r_0aEL}{r_0^2 r} \\ &\quad + \frac{-L^2 + 2r_0M + r_0^2E^2}{r_0^2}. \end{aligned} \tag{95}$$

Note that the particle can exist only in regions where $R(r) \geq 0$. Also, note that at the horizon $R(r_+) \geq 0$ and $R(r_+) = 0$ for a particle with the critical momentum $L_c = r_0 r_+ E/a$. Therefore, from expression (95), we find that if $2ML^2 - r_0a^2 - 2r_0aEL > 0$ the radial function has the asymptotic behaviors $R(r \to \infty) \to -\infty$ and $R(r \to 0) \to \infty$, so the function $R(r)$ has only one positive root, say r_*^+; thus, the particle can exist only in the region $0 < r < r_*$. On the other hand, if $2ML^2 - r_0a^2 - 2r_0aEL < 0$, we find $R(r \to \infty) \to -\infty$ and $R(r \to 0) \to -\infty$, so the function $R(r)$ has two positive roots, and the particle can exist in the region between the roots. The roots of $R(r)$ are given by

$$r_*^{\pm} = \frac{E^2r_0^2 + 2Mr_0 - L^2 \pm \sqrt{8r_0ML^2 - 4a^2r_0^2 - 8ar_0^2LE + (E^2r_0^2 + 2Mr_0 - L^2)^2}}{2r_0}. \tag{96}$$

For a particle with the critical angular momentum, the radial function is given by

$$R^c = R(r)|_{L=L_c} = \frac{r - r_+}{r}\left(-\frac{r - r_-}{r_0} + \frac{E^2(a^2 - r_+^2)}{a^2}\right), \tag{97}$$

and it vanishes on the event horizon; to simplify the above equation, we have used $r_+r_- = a^2$.

The roots of the radial function $R(r)|_{L=L_c}$ are given by

$$\begin{aligned} r_1 &= r_+ \\ r_2 &= r_- + \frac{r_0E^2(a^2 - r_+^2)}{a^2}. \end{aligned} \tag{98}$$

Particles with critical angular momentum can reach the event horizon if

$$\left.\frac{dR^c}{dr}\right|_{r=r_+} > 0. \tag{99}$$

TABLE I. The behavior of $\frac{E^2_{\text{c.m.}}}{2m_0}$ as a function of L_1 for $a = 1.9$, $M = 2$, $r_0 = 1$, $E_1 = 1$, $E_2 = 2$, and $L_2 = 3$. The critical angular momentum is given by $L_c = \frac{E_1 r_0 r_-}{a} = 0.723947$.

L_1	$\frac{E^2_{\text{c.m.}}}{2m_0}$	L_1	$\frac{E^2_{\text{c.m.}}}{2m_0}$
5.0	3.97	0.73	177.32
4.0	3.23	0.729	212.36
3.0	2.56	0.728	264.71
2.0	2.12	0.727	351.34
1.0	4.34	0.726	522.40
0.9	6.47	0.725	1018.50
0.8	14.39	0.724	20 404.30
0.75	41.40	0.72 395	424 247.95
0.74	67.02	0.723 948	2.03×10^6

For the linear dilaton black hole, we obtain

$$\left.\frac{dR^c}{dr}\right|_{r=r_+} = -\frac{(r_+ - r_-)(1 + r_0 r_+ E^2/a^2)}{r_0 r_+} < 0; \quad (100)$$

therefore, if particles with critical angular momentum exist outside the black hole, they cannot reach the event horizon. In Fig. 12, we plot the behavior of R^c as a function of r for the nonextremal linear dilaton black hole. Notice that if $\frac{d^2R^c}{dr^2}|_{r=r_+} = 2(\frac{E^2}{a^2} - \frac{E^2}{r_+^2} - \frac{r_-}{r_0 r_+^2}) < 0$ then r_2 is positive and smaller than r_- and if $\frac{d^2R^c}{dr^2}|_{r=r_+} = 2(\frac{E^2}{a^2} - \frac{E^2}{r_+^2} - \frac{r_-}{r_0 r_+^2}) > 0$ then r_2 is negative; therefore, particles with critical angular momentum cannot exist outside the event horizon.

On the other hand, we notice that the particle with the critical angular momentum can exist inside the event horizon r_+. This can be shown by replacing the critical angular momentum (93) in the square of the radial component of the 4-velocity (84), obtaining the analog of Eq. (97), of which the derivative evaluated on the internal horizon r_- is positive $\frac{dR^c}{dr}|_{r=r_-} > 0$; therefore, the particle with critical angular momentum can reach the inner horizon, and the c.m. energy can be arbitrarily high, with the BSW process being possible on the inner horizon. This behavior is similar to the rotating Bañados-Teitelboim-Zanelli (BTZ) black hole [35–37]. In Table I, we show the behavior of the c.m. energy on the inner horizon as a function of the angular momentum L_1 of a particle, and we observe that when L_1 approaches the critical angular momentum $L_c = \frac{r_0 r_- E}{a}$ the c.m. energy increases and tends to infinity when $L_1 \to L_c$. Also, in Table II, we show the critical angular momentum $L_c = \frac{E_1 r_0 r_-}{a}$ and $e^{-2\phi}(r)$ for different values of r_0. Notice that in the equatorial plane the string coupling depends on r_0 and it does not depend on a. We also observe that when the coupling r_0 is increasing the string coupling becomes stronger and this leads to a higher value of the critical angular momentum. Thus, a strong string coupling requires the particle to have a high angular momentum in the collision process in order for the rotating linear dilaton black hole to act as a particle accelerator.

TABLE II. Critical angular momentum $L_c = \frac{E_1 r_0 r_-}{a}$ and $e^{-2\phi}(r)$ for different values of r_0, for $a = 1.9$, $M = 2$, and $E_1 = 1$.

r_0	$e^{-2\phi}(r)$	L_c
0.5	$\frac{1}{2r}$	0.263
1.0	$\frac{1}{r}$	0.526
1.5	$\frac{3}{2r}$	0.789
2.0	$2r$	1.053

On the other hand, in the extremal case, the function $R^c(r)$ for a particle with critical angular momentum reads

$$R^c(r) = -\frac{(r - M)^2}{r_0 r}. \quad (101)$$

So, the function $R^c(r)$ is null for $r = r_+ = M$, which is the degenerate horizon of the extremal black hole. Notice that the particle with critical angular momentum cannot exist outside the event horizon; however, it can exist on the degenerate horizon, which is similar to the behavior for the extremal BTZ black hole [35–37].

Now, in order to illustrate these behaviors, we show some graphics. In Fig. 10, we have plotted the behavior of

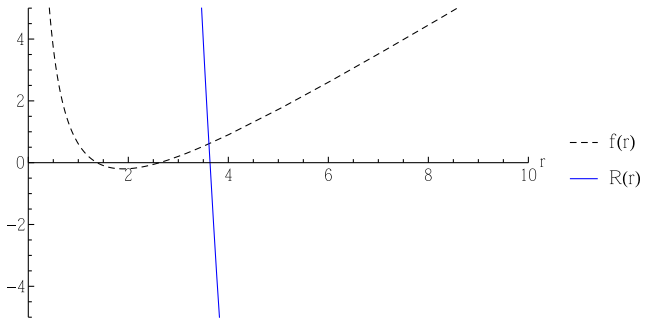

FIG. 10. The behavior of $f(r)$ and $R(r)$ for $a = 1.9$, $M = 2$, $r_0 = 1$, $E = 1$, and $L = 10$.

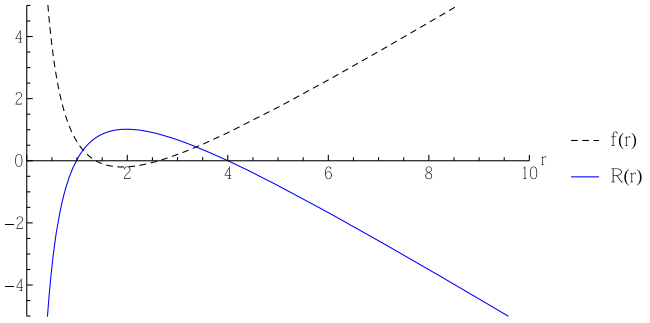

FIG. 11. The behavior of $f(r)$ and $R(r)$ for $a = 1.9$, $M = 2$, $r_0 = 1$, $E = 1$, and $L = 0.1$.

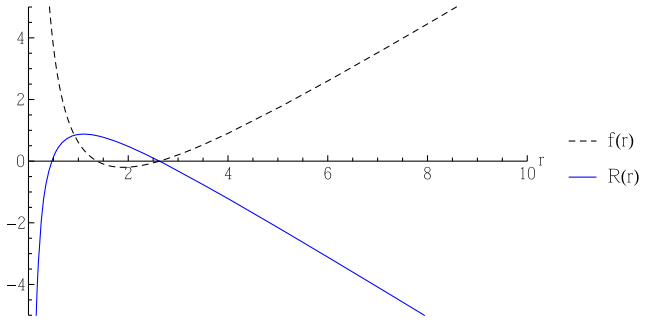

FIG. 12. The behavior of $f(r)$ and $R(r)$ for $a = 1.9$, $M = 2$, $r_0 = 1$, $E = 1$, and $L = L_c$.

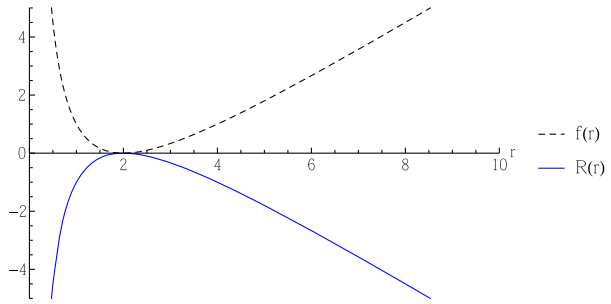

FIG. 13. The behavior of $f(r)$ and $R(r)$ for $a = 2$, $M = 2$, $r_0 = 1$, $E = 1$, and $L = L_c$.

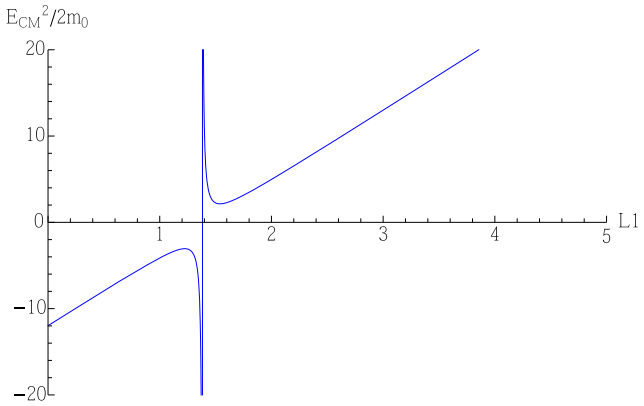

FIG. 14. The behavior of $E_{\text{c.m.}}$ as a function of L_1, for $a = 1.9$, $M = 2$, $r_0 = 1$, $E_1 = 1$, $E_2 = 2$, and $L_2 = 3$.

$f(r)$ and $R(r)$ for $a = 1.9$, $M = 2$, $r_0 = 1$, $E = 1$, and $L = 10$, and in Fig. 11, we have plotted the behavior of $f(r)$ and $R(r)$ for $a = 1.9$, $M = 2$, $r_0 = 1$, $E = 1$, and $L = 0.1$. In Figs. 12 and 13, we show the behavior of $R^c(r)$ for a particle with critical angular momentum in the nonextremal and in the extremal cases, respectively. One root of $R^c(r)$ coincides with the horizon in the nonextremal case. This means that the particle with the critical angular momentum can exist inside the outer horizon and the particle collision on the inner horizon could produce arbitrarily high c.m. energy. In the extremal case, the roots

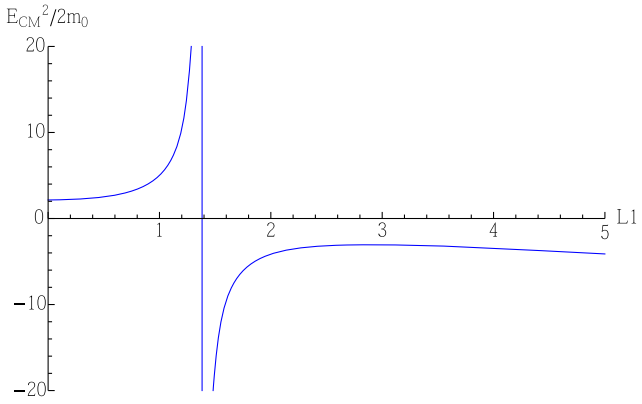

FIG. 15. The behavior of $E_{\text{c.m.}}$ as a function of L_1, for $a = 1.9$, $M = 2$, $r_0 = 1$, $E_1 = 1$, $E_2 = 2$, and $L_2 = 0.5$.

of $R^c(r)$ coincide with the degenerate horizon, so particles with critical angular momentum can only exist on the degenerate horizon.

In Fig. 14, we have plotted the behavior of $E_{\text{c.m.}}$ as a function of L_1, with $a = 1.9$, $M = 2$, $r_0 = 1$, $E_1 = 1$, $E_2 = 2$, and $L_3 = 3$. We see that in order to get infinite c.m. energy, particle 1 reaches the critical angular momentum as shown in Figs. 14 and 15.

VI. GENERAL EQUATIONS OF GEODESIC MOTION

In this section, we solve analytically the geodesic equations of motion of the test particle for the radial, temporal, and orbital motion.

A. Analysis of the angular motion (θ-motion)

In order to study the θ-motion, we consider the equation of motion (27), which can be rewritten as $d\theta/d\gamma = \sqrt{\Theta}$, where the coordinate θ is a polar angle that can take only positive values. So,

$$\Theta = k^2 - \frac{L^2}{\sin^2\theta} \geq 0, \tag{102}$$

where the separability constant is non-null or negative. Now, through the change of variable $\xi = \cos\theta$, Eq. (27) yields

$$\frac{d\xi}{d\gamma} = -\sqrt{\Theta_\xi}, \tag{103}$$

being $\Theta_\xi = k^2(1-\xi^2) - L^2$. The roots of the function Θ_ξ are given by

$$\theta_1 = \arccos\left(\sqrt{1-\frac{L^2}{k^2}}\right), \qquad \theta_2 = \arccos\left(-\sqrt{1-\frac{L^2}{k^2}}\right), \tag{104}$$

which define the cone's angles that confine the movement of the particle. Integrating (103), we get

$$\gamma(\xi) = -\int \frac{d\xi}{\sqrt{k^2(1-\xi^2)-L^2}}. \tag{105}$$

The solution, in terms of the variable θ, is

$$\gamma(\theta) = \frac{1}{\sqrt{k^2}}\arccos\left(\frac{\cos\theta}{\sqrt{1-\frac{L^2}{k^2}}}\right), \tag{106}$$

where we have used that $\gamma_0 = 0$ for $\theta_0 = \theta_1$. Also, the above equation can be inverted, which yields

$$\theta(\gamma) = \arccos\left(\sqrt{1-\frac{L^2}{k^2}}\cos(\sqrt{k^2}\gamma)\right) \tag{107}$$

for $k^2 > L^2$.

B. Analysis of the radial motion (*r*-motion)

Now, we consider the motion of the particle with respect to the r-coordinate. We will focus on Eq. (28) in order to obtain the radial velocity of the particle dr/dt. The condition of turning point $(\frac{dr}{dt})_{r=r_t} = 0$ allows us to define an effective potential,

$$\left(E-\frac{aL}{r_0 r}\right)^2 - f(r)\left(m^2+\frac{k^2}{r_0 r}\right) = (E-V_-)(E-V_+), \tag{108}$$

where we can recognize the effective potential for the particle with mass m as

$$V_\pm = \frac{aL}{r_0 r} \pm \sqrt{f(r)\left(m^2+\frac{k^2}{r_0 r}\right)}. \tag{109}$$

The behavior of the effective potential is shown in Fig. 1. In the following sections, we will consider the motion of particles $m \neq 0$ and the motion of photons $m = 0$ separately.

1. Radial motion of particles

Now, Eq. (28) can be written as

$$\left(\frac{dr}{d\gamma}\right)^2 = P(r), \tag{110}$$

where $P(r) = -a_3 r^3 + a_2 r^2 + a_1 r + a_0$, with

$$\begin{aligned} a_0 &= -a^2(k^2-L^2), \quad a_1 = 2k^2M - 2aELr_0 - a^2m^2r_0, \\ a_2 &= -k^2 + 2m^2Mr_0 + E^2r_0^2, \quad a_3 = m^2r_0 > 0. \end{aligned} \tag{111}$$

Integrating the above equation, where r_1 corresponds to the starting point, we obtain

$$\int_{\gamma_i=0}^{\gamma} d\gamma = \frac{1}{\sqrt{a_3}}\int_{r_1}^{r}\frac{-dr}{\sqrt{P(r)/a_3}}, \tag{112}$$

with the change of variable $r = -4x + \frac{a_2}{3a_3}$, and the integral transforms to

$$\gamma(r) = \frac{1}{\sqrt{a_3}}\int_{x_1}^{x}\frac{dx}{\sqrt{4x^3 - g_2 x - g_3}}, \tag{113}$$

where $r_1 = -4x_1 + \frac{a_2}{3a_3}$. The invariants are

$$\begin{aligned} g_2 &= \frac{1}{a_3}\left(\frac{a_2^2}{3a_3} + a_1\right), \\ g_3 &= -\frac{1}{16a_3}\left(a_0 + \frac{2a_2^3}{27a_3^2} + \frac{a_1a_2}{3a_3}\right), \end{aligned} \tag{114}$$

$$\gamma = \frac{1}{\sqrt{a_3}}(\wp^{-1}(x; g_2, g_3) - \varphi_1), \tag{115}$$

with $\varphi_1 = \wp^{-1}(x_1; g_2, g_3)$. Inverting this expression, we obtain

$$r(\gamma) = \frac{a_2}{3a_3} - 4\wp(\sqrt{a_3}\gamma + \varphi_1; g_2, g_3). \tag{116}$$

2. Bounded radial motion of photons

For photons falling from ρ_1,

$$\int_0^{\gamma} d\gamma = \frac{1}{\sqrt{b_2}}\int_{\rho_1}^{r}\frac{-dr}{\sqrt{P_2(r)/b_2}}, \tag{117}$$

where $P_2(r) = -b_2 r^2 + b_1 r - b_0$, and

$$\begin{aligned} b_0 &= a^2(k^2-L^2), \qquad b_1 = 2k^2M - 2aELr_0, \\ b_2 &= k^2 - E^2r_0^2, \qquad b_4 = b_1^2 - 4b_0b_2, \end{aligned} \tag{118}$$

$$\gamma = \frac{1}{\sqrt{b_2}}\left(\arcsin\left(\frac{b_1 - 2b_2 r}{\sqrt{b_4}}\right) - \varphi_2\right), \tag{119}$$

with $\varphi_2 = \arcsin(\frac{b_1 - 2b_2\rho_1}{\sqrt{b_4}})$. Inverting this expression, we obtain

$$r(\gamma) = \frac{b_1}{2b_2} - \frac{\sqrt{b_4}}{2b_2}\sin(\sqrt{b_2}\gamma + \varphi_2). \tag{120}$$

3. Unbounded radial motion of photons

In this case, we will consider $E = k/r_0$, and the solution is given by

$$r(\gamma) = \frac{b_0}{c_1} + \frac{1}{c_1}\left(\varphi_3 \pm \frac{c_1}{2}\gamma\right)^2, \tag{121}$$

where $c_1 = 2k(Mk - aL)$, $\varphi_3 = \sqrt{c_1\rho_1 - b_0}$, and the plus sign corresponds to photons that escape to infinity and the minus sign corresponds to photons that fall into the horizon.

C. Analysis of the angular motion (φ-motion)

From Eq. (25), it is possible to distinguish an integral in the radial part and one in the angular θ part; so, the solution can be written as $\varphi = \varphi^m(r) + \varphi(\theta)$. The solution of the angular integral is given by

$$\varphi(\theta) = \frac{\pi}{2} + \frac{1}{2}\arcsin\left[\frac{\cos^2\theta_1 - \cos\theta}{\cos\theta_1(1-\cos\theta)}\right] - \frac{1}{2}\arcsin\left[\frac{\cos^2\theta_1 + \cos\theta}{\cos\theta_1(1+\cos\theta)}\right], \tag{122}$$

and for particles, the radial integral yields

$$\varphi^{m=1}(r) = \frac{a\sqrt{r_0}E}{4m(r_+ - r_-)}\left[\left(r_+ - \frac{aL}{r_0E}\right)(\bar{F}_+(u_1) - \bar{F}_+(u)) - \left(r_- - \frac{aL}{r_0E}\right)(\bar{F}_-(u_1) - \bar{F}_-(u))\right], \tag{123}$$

where

$$\bar{F}_\pm(r) = \frac{2\zeta(W_\pm)\wp^{-1}[u(r)]}{\wp'(W_\pm)} + \frac{1}{\wp'(W_\pm)}\ln\left|\frac{\sigma[\wp^{-1}[u(r)] - W_\pm]}{\sigma[\wp^{-1}[u(r)] + W_\pm]}\right|, \tag{124}$$

$$u(r) = \frac{a_2}{12a_3} - \frac{r}{4}, \tag{125}$$

$u_1 = u(r_1)$ and

$$W_\pm = \wp^{-1}\left[\frac{a_2}{12a_3} - \frac{r_\pm}{4}\right]. \tag{126}$$

On the other hand, for bounded photons, the solution is

$$\varphi^{m=0}(r) = \frac{ar_0E}{\sqrt{b_2}(r_+ - r_-)}\left[\left(r_+ - \frac{aL}{r_0E}\right)(\bar{G}_+(r) - \bar{G}_+(\rho_1)) - \left(r_- - \frac{aL}{r_0E}\right)(\bar{G}_-(r) - \bar{G}_-(\rho_1))\right], \tag{127}$$

with

$$\bar{G}_\pm(r) = +\frac{1}{\sqrt{\gamma_\pm}}\cosh^{-1}\left|\frac{2\gamma_\pm + \delta_\pm(r - r_\pm)}{(r - r_\pm)\sqrt{4\gamma_\pm + \delta_\pm^2}}\right|, \tag{128}$$

and

$$\gamma_\pm = \frac{b_1}{b_2}r_\pm - \frac{b_0}{b_2} - r_\pm^2,$$
$$\delta_\pm = \frac{b_0}{b_2} - 2r_\pm,$$

while for unbounded photons, the solution is

$$\varphi^{(0)}(r) = \frac{ar_0E}{(r_+ - r_-)}\left[\left(r_+ - \frac{aL}{r_0E}\right)(\bar{J}_+(r) - \bar{J}_+(\rho_1)) - \left(r_- - \frac{aL}{r_0E}\right)(\bar{J}_-(r) - \bar{J}_-(\rho_1))\right], \tag{129}$$

where

$$\bar{J}_\pm(r) = \frac{2}{\sqrt{b_0 - c_1r_\pm}}\tan^{-1}\left|\frac{\sqrt{c_1r - b_0}}{\sqrt{b_0 - c_1r_\pm}}\right|. \tag{130}$$

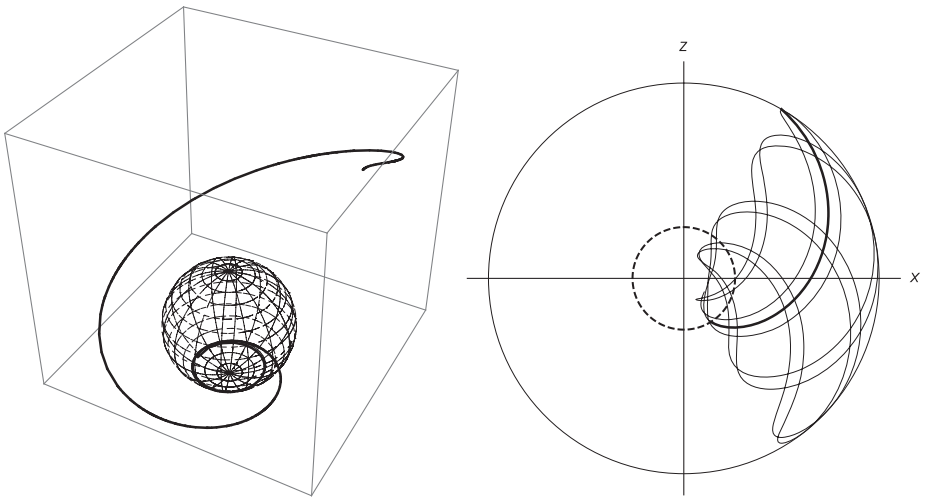

FIG. 16. Trajectory for a particle that falls into the horizon. The left figure is for three-dimensional motion, and the right figure is for the motion in the r-θ plane, for $a = 1.9$, $M = 2$, $r_0 = 1$, $r_1 = 10$, $k = 4$, and $L = 2$.

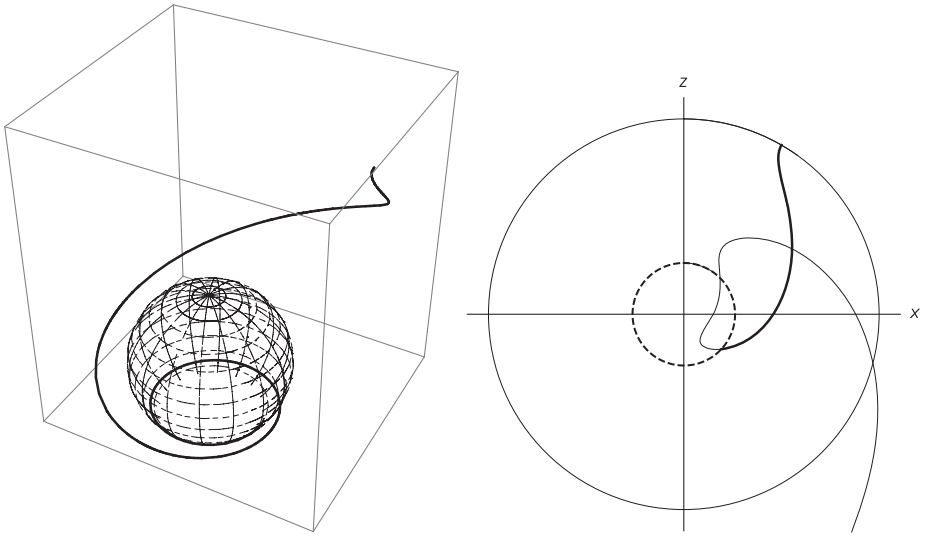

FIG. 17. Trajectory for a photon that falls into the horizon. The left figure is for three-dimensional motion, and the right figure is for the projection of the orbit onto the x-z plane, for $a = 1.9$, $M = 2$, $r_0 = 1$, $\rho_1 = 10$, $k = 4$, and $L = 2$.

D. Analysis of the time motion (*t*-motion)

The solution for the *t*-motion of particles is given by the following expression,

$$t^{(m=1)}(r) = \frac{a\sqrt{r_0}E}{r_-}\left[\wp^{-1}(u) - \wp^{-1}(u_A) + \frac{r_+}{4}[\bar{F}_+(u_A) - \bar{F}_+(u)]\right], \tag{131}$$

where we have considered by simplicity that the energy of the particle is $E_A = V(r_-) = V(R_A) = aL/r_0 r_-$, with R_A being the turning point or apoastron and $u_A = u(R_A)$. On the other hand, the solution for the *t*-motion of bounded photons yields

$$t^{(m=0)}(r) = \frac{ar_0 E}{r_-\sqrt{b_2}}\left[\arcsin\left(\frac{b_1 - 2b_2 r}{\sqrt{b_4}}\right) - \arcsin\left(\frac{b_1 - 2b_2\rho_A}{\sqrt{b_4}}\right) + \frac{r_+}{\sqrt{\gamma_+}}[\bar{G}_+(r) - \bar{G}_+(\rho_A)]\right], \tag{132}$$

where we have considered for simplicity that the energy of the photon is $E_A = V(r_-) = V(\rho_A) = aL/r_0 r_-$, with ρ_A

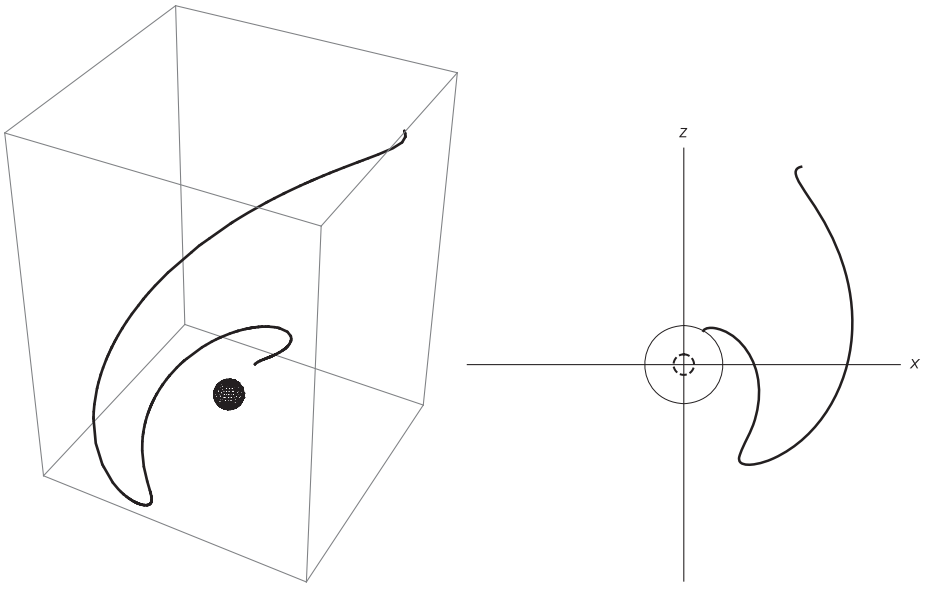

FIG. 18. Trajectory for a photon that escapes to infinity. The left figure is for three-dimensional motion, and the right figure is for the projection of the orbit onto the x-z plane, for $a = 1.9$, $M = 2$, $k = 4$, $L = 10$, and $\rho_1 = 10$.

being the turning point or apoastron, while for unbounded photons, the solution of the t-motion is given by

$$t^{(0)}(r) = \pm\frac{ar_0E}{r_-}\left[\frac{2}{c_1}[\sqrt{c_1r-b_0}-\sqrt{c_1\rho_A-b_0}] + r_+[\bar{J}_+(r)-\bar{J}_+(\rho_A)]\right], \tag{133}$$

where we have considered for simplicity that the energy of the photon is $E_A = V(r_-) = V(\rho_A) = aL/r_0r_-$ and $k = aL/r_-$, with ρ_A being the starting point of the trajectory.

Now, in order to show the trajectories for particles and photons, we plot in Fig. 16 the trajectory of a particle that falls into the black hole (left figure) and the motion in the r-θ plane (right figure). Then, in Fig. 17, we plot the trajectory of a photon that falls into the black hole (left figure) and the motion in the r-θ plane (right figure). Finally, in Fig. 18, we plot the trajectory of a photon that escapes to spatial infinity (left figure) and the motion in the r-θ plane (right figure).

VII. SUMMARY

In this paper, we studied the motion of particles in a linear dilaton black hole background. We analyzed the motion of particles in the equatorial plane as well as in four dimensions analytically. Mainly, a qualitative analysis of the effective potential for null geodesics shows that photons plunge into the horizon or escape to infinity; they are not deflected. The study for massive particles shows that there are not confined orbits of the first kind, like planetary or circular orbit. Therefore, the r-motion is not periodic, and it is not possible to define the orbital frequencies, Ω_r, Ω_θ, and Ω_ϕ, that determine the perihelion shift and the Lense-Thirring effects, which are defined as differences between these orbital frequencies. Now, considering the θ-motion, we observe that the polar coordinate is confined to oscillate between θ_1 and θ_2. The θ-motion is periodic with a period

$$\omega_\theta = 2\gamma(\theta_2) = \frac{2\pi}{k}, \tag{134}$$

and the corresponding frequency is $2\pi/\omega_\theta$. The secular accumulation rates of the angle ϕ are given by

$$Y_\phi^{(m)} = \frac{2}{\omega_\theta}\phi(\theta_2) = \frac{2}{\omega_\theta}[\varphi^m(\theta_2)+\varphi(\theta_2)] = \frac{k}{\pi}[\varphi^m(\theta_2)+\pi], \tag{135}$$

where $\varphi^m(\theta_2) = \varphi^m[r^m(\frac{\pi}{k})]$ and $\gamma(\theta_2) = \frac{\pi}{k}$. The secular accumulation rates of the angle ϕ are different for particles and photons. It is worth mentioning that another remarkable feature of the motion of photons is the existence of circular orbits of any radius. This occurs in the extremal case ($M = a$) and for $L = Er_0$.

Also, we analyzed the collision of particles near the horizon, and we studied the possibility that the dilaton black hole acts as a particle accelerator. We found that when one of the particles with critical angular momentum, which exists inside the outer horizon, collides with another particle it can produce an arbitrarily high c.m. energy, in the nonextremal case. For the extremal case, we have found that the particles with critical angular momentum can only exist on the degenerate horizon. The above arguments show that the motion and collision of particles in the linear dilaton black hole have a behavior similar to that of motion and collision of particles in the BTZ black hole [35–37,44]. Also, we showed that in the equatorial plane the string coupling depends on r_0, and it does not depend on a. Then, we observed that when the coupling r_0 is increasing the string coupling becomes stronger, and this leads to a higher value of the critical angular momentum. Thus, a strong string coupling requires the particle to have a high angular momentum in the collision process in order for the rotating linear dilaton black hole to act as a particle accelerator.

ACKNOWLEDGMENTS

This work was partially funded by the Comisión Nacional de Ciencias y Tecnología through FONDECYT Grant No. 11140674 (P. A. G.) and by the Dirección de Investigación y Desarrollo de la Universidad de La Serena (Y. V.). P. A. G. acknowledges the hospitality of the Universidad de La Serena and National Technical University of Athens, and E. P. and Y. V. acknowledge the hospitality of the Universidad Diego Portales, where part of this work was carried out.

[1] G. W. Gibbons and K. i. Maeda, Black holes and membranes in higher dimensional theories with dilaton fields, Nucl. Phys. **B298**, 741 (1988).
[2] D. Garfinkle, G. T. Horowitz, and A. Strominger, Charged black holes in string theory, Phys. Rev. D **43**, 3140 (1991); Erratum, Phys. Rev. D **45**, 3888 (1992).
[3] A. Sen, Rotating Charged Black Hole Solution in Heterotic String Theory, Phys. Rev. Lett. **69**, 1006 (1992).
[4] A. Sen, Black hole solutions in heterotic string theory on a torus, Nucl. Phys. **B440**, 421 (1995).
[5] S. F. Hassan and A. Sen, Twisting classical solutions in heterotic string theory, Nucl. Phys. **B375**, 103 (1992).

[6] R. R. Khuri, Solitons, black holes and duality in string theory, Nucl. Phys. B, Proc. Suppl. **61A**, 99 (1998).

[7] C. J. Gao and S. N. Zhang, Topological black holes in dilaton gravity theory, Phys. Lett. B **612**, 127 (2005).

[8] G. Clement, D. Gal'tsov, and C. Leygnac, Linear dilaton black holes, Phys. Rev. D **67**, 024012 (2003).

[9] I. Sakalli, Analytical solutions in rotating linear dilaton black holes: Resonant frequencies, quantization, greybody factor, and Hawking radiation, Phys. Rev. D **94**, 084040 (2016).

[10] I. Sakalli and G. Tokgoz, Stationary scalar clouds around maximally rotating linear dilaton black holes, Classical Quantum Gravity **34**, 125007 (2017).

[11] S. W. Hawking and H. S. Reall, Charged and rotating AdS black holes and their CFT duals, Phys. Rev. D **61**, 024014 (1999).

[12] R. Li, Analytical studies of Hawking radiation and quasi-normal modes in rotating linear dilatonic black hole, Eur. Phys. J. C **73**, 2296 (2013).

[13] S. Fernando, Null geodesics of charged black holes in string theory, Phys. Rev. D **85**, 024033 (2012).

[14] S. Soroushfar, R. Saffari, and E. Sahami, Geodesic equations in the static and rotating dilaton black holes: Analytical solutions and applications, Phys. Rev. D **94**, 024010 (2016).

[15] T. Maki and K. Shiraishi, Motion of test particles around a charged dilatonic black hole, Classical Quantum Gravity **11**, 227 (1994).

[16] M. Olivares and J. R. Villanueva, Massive neutral particles on heterotic string theory, Eur. Phys. J. C **73**, 2659 (2013).

[17] C. Blaga, Circular time-like geodesics around a charged spherically symmetric dilaton black hole, Applications Math. **22**, 41 (2013).

[18] C. Blaga, Timelike geodesics around a charged spherically symmetric dilaton black hole, Serb. Astron. J. **190**, 41 (2015).

[19] J. R. Villanueva and M. Olivares, Gravitational Rutherford scattering and Keplerian orbits for electrically charged bodies in heterotic string theory, Eur. Phys. J. C **75**, 562 (2015).

[20] P. A. Gonzalez, M. Olivares, E. Papantonopoulos, J. Saavedra, and Y. Vasquez, Motion of magnetically charged particles in a magnetically charged stringy black hole spacetime, Phys. Rev. D **95**, 104052 (2017).

[21] M. Bañados, J. Silk, and S. M. West, Kerr Black Holes as Particle Accelerators to Arbitrarily High Energy, Phys. Rev. Lett. **103**, 111102 (2009).

[22] A. A. Grib and Y. V. Pavlov, Particles with negative energies in black holes, Int. J. Mod. Phys. D **20**, 675 (2011).

[23] O. B. Zaslavskii, Acceleration of particles as universal property of rotating black holes, Phys. Rev. D **82**, 083004 (2010).

[24] O. B. Zaslavskii, Acceleration of particles by nonrotating charged black holes, Pis'ma Zh. Eksp. Teor. Fiz. **92**, 635 (2010) [JETP Lett. **92**, 571 (2010)].

[25] F. Hejda and J. Bičák, Kinematic restrictions on particle collisions near extremal black holes: A unified picture, Phys. Rev. D **95**, 084055 (2017).

[26] S. Gao and C. Zhong, Non-extremal Kerr black holes as particle accelerators, Phys. Rev. D **84**, 044006 (2011).

[27] Y. Li, J. Yang, Y. L. Li, S. W. Wei, and Y. X. Liu, Particle acceleration in Kerr-(anti-)de Sitter black hole backgrounds, Classical Quantum Gravity **28**, 225006 (2011).

[28] O. B. Zaslavsky, Acceleration of particles as a universal property of ergosphere, Mod. Phys. Lett. A **28**, 1350037 (2013).

[29] A. Abdujabbarov, N. Dadhich, B. Ahmedov, and H. Eshkuvatov, Particle acceleration around a five-dimensional Kerr black hole, Phys. Rev. D **88**, 084036 (2013).

[30] U. Debnath, Particles Collision near Kerr-Sen Dilaton-Axion Black Hole, arXiv:1508.02385.

[31] O. B. Zaslavskii, Black hole with a scalar field as a particle accelerator, Int. J. Mod. Phys. D **26**, 1750108 (2017).

[32] J. Sadeghi, B. Pourhassan, and H. Farahani, Rotating charged hairy black hole in $(2+1)$ dimensions and particle acceleration, Commun. Theor. Phys. **62**, 358 (2014).

[33] S. Fernando, Spinning dilaton black hole in $2+1$ dimensions as a particle accelerator, Mod. Phys. Lett. A **32**, 1750074 (2017).

[34] R. Becar, P. A. Gonzalez, and Y. Vasquez, Particle collisions near a three-dimensional warped AdS black hole, arXiv:1712.00868.

[35] K. Lake, Particle Accelerators inside Spinning Black Holes, Phys. Rev. Lett. **104**, 211102 (2010); Erratum, Phys. Rev. Lett. **104**, 259903 (2010).

[36] J. Yang, Y. L. Li, Y. Li, S. W. Wei, and Y. X. Liu, Particle collisions in the lower dimensional rotating black hole space-time with the cosmological constant, Adv. High Energy Phys. **2014**, 204016 (2014).

[37] N. Tsukamoto, K. Ogasawara, and Y. Gong, Particle collision with an arbitrarily high center-of-mass energy near a Baados-Teitelboim-Zanelli black hole, Phys. Rev. D **96**, 024042 (2017).

[38] S. Fernando, String black hole: Can it be a particle accelerator?, Gen. Relativ. Gravit. **46**, 1634 (2014).

[39] S. B. Giddings and A. Strominger, Dynamics of extremal black holes, Phys. Rev. D **46**, 627 (1992).

[40] A. H. H. Hamo and I. Sakalli, Exact solutions to the geodesic equations of linear dilaton black holes, Turk. J. Phys. **40**, 139 (2016).

[41] S. Chandrasekhar, *The Mathematical Theory of Black Holes* (Oxford University, New York, 1983).

[42] N. Deruelle and R. Ruffini, Quantum and classical relativistic energy states in stationary geometries, Phys. Lett. **52B**, 437 (1974).

[43] B. Shutz, *A First Course in General Relativity* (Cambridge University Press, New York, 2009).

[44] N. Cruz, C. Martinez, and L. Pena, Geodesic structure of the $(2+1)$ black hole, Classical Quantum Gravity **11**, 2731 (1994).